Control Design and Analysis of a Capturing Device Performing In-Air Capturing of a Reusable Launch Vehicle

Sunayna Singh[1]*, Madalin Simioana[2], Sven Stappert[1], Martin Sippel[1],
Sophia Buckingham[3], Silvania Lopes[3] and Yakut Cansev Kucukosman[3]

[1]DLR Institut für Raumfahrtsysteme, Bremen, Germany
**Linzer Strasse 1, 28359, Bremen, Sunayna.Singh@dlr.de*

[2]Astos Solutions, Romania
Blvd. Alexandru Ioan Cuza 32a, 011055, Bucharest, madalin.simioana@astos.ro

[3]von Karman Institute for Fluid Dynamics VKI, Belgium
72 Chaussée de Waterloo, Rhode-St-Genèse B-1640, sophia.buckingham@vki.ac.be

Abstract

The innovative 'In-Air-Capturing (IAC)' recovery method involves winged rocket stages being captured mid-air and towed back to the launch site. This patented approach by German Aerospace Center (DLR), shows potential for substantial cost reduction by eliminating the need for an additional propulsion system during descent. An important operation in IAC involves a capturing device attached to a rope, which is released from a towing aircraft. This device must autonomously navigate its way to the winged launcher stage in the vicinity of the aircraft. This process known as capture phase of 'In-Air Capturing' is expected to last about 70 s. The device must overcome disturbing forces originating from the flexible rope and wake of the aircraft to establish connection with the launcher stage. This paper studies the modelling and simulation of the capture phase. The main focus lies on the flexible dynamics of the rope and the control of the capturing device. First, extensive sensitivity studies are performed to select the best configuration for the rope. Then, a robust feedback controller including active damping is proposed to mitigate the vibrations from the rope and allow the capturing device to maneouvre with agility and accuracy. Using open loop tests, it is confirmed that the system remains stable. The rope is also proved to be strong enough to support the towing loads from pulling a large launcher stage. Closed loop tests show that the device is able to perform multiple maneouvres within the capture window. However, the device was unable to maneouvre when exposed to the strong regions of wake. A longer rope is proposed to mediate the effect of wake in future simulations.

1. Introduction

In the recent years, the development of multiple reusable launch systems has provided a means to achieve higher launch frequencies while keeping the costs in check. The recovery methods that are widely studied and utilized are mainly Vertical Take-off Vertical Landing (VTVL) and Vertical Take-Off Horizontal Landing (VTHL). However, some other non-conventional recovery methods, like partial recovery of launcher parts using inflatable devices and capture of rocket stages with helicopters (mid-air retrieval) have also shown scope for cost savings. One such innovative method, called 'In-Air Capturing (IAC)' has been proposed by DLR [1]. The idea involves 'the winged stage being caught mid-air using an aircraft and towed back to the launch site without the need of additional propulsion system for landing' [2] . This provides potential for considerable cost reduction as the propulsion system is one of the most expensive components of a launch vehicle [3].

The operational cycle of IAC starts with the launcher lifting off vertically and ascending until Main Engine Cut-Off (MECO). At MECO, the winged first stage separates from the launch vehicle and re-enters the atmosphere in a ballistic trajectory, in the course of which it decelerates from supersonic velocity to a subsonic glide. Meanwhile, a capturing aircraft is waiting at the downrange rendezvous area, loitering until the Reusable Launch Vehicle (RLV) arrives. Between 8 km to 2 km altitude, the final IAC manoeuvre is performed [4]. To get a better understanding of the IAC manoeuvre, the process can be divided into five phases as shown in Figure 1:

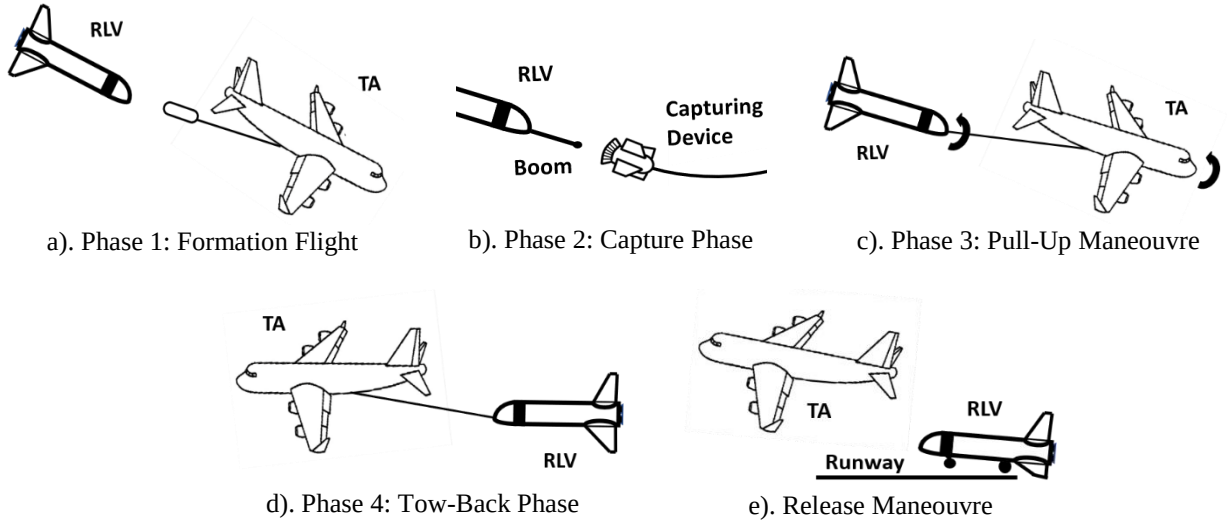

a). Phase 1: Formation Flight b). Phase 2: Capture Phase c). Phase 3: Pull-Up Maneouvre

d). Phase 4: Tow-Back Phase e). Release Maneouvre

Figure 1: Phases of In-Air Capturing Manoeuvre

- *Phase 1: Formation Flight*
  During the *formation flight phase* (Figure 1a), an unpowered Towing Aircraft (TA) glides from cruise flight and attempts to achieve a parallel descending formation with the RLV. Here, both vehicles attempt to maintain similar velocities and flight path angles, while separated by a safe distance (between 150 m to 350 m). The formation envelope must be maintained long enough for the *capture phase* to be successfully completed. A detailed analysis of the dynamics and trajectories of this phase can be found in [5].

- *Phase 2: Capture Phase*
  While the two vehicles are in formation, the *capture phase* (Figure 1b) is carried out. A capturing device attached to a rope is first released from the aircraft. This agile device autonomously navigates its way to the RLV and ensures mating of the two vehicles. Once the RLV is connected to the TA via the rope, the aircraft acts like an external propulsion system to the RLV. A detailed modelling of critical aspects like aerodynamics, rope dynamics and control architecture of this phase has been discussed in [6] and [7].

- *Phase 3: Pull-Up Manoeuvre*
  Next the mated configuration in descending flight performs a *pull-up manoeuvre* (Figure 1c) to transition to an ascending flight. During this, the TA engines are turned on to provide thrust to the system. The configuration can then gain altitude and achieve a suitable cruise state. This phase has been examined in [8].

- *Phase 4: Tow-Back Phase*
  The *tow-back flight* (Figure 1d) simply involves the TA towing the RLV to the landing site. The configuration flies at an optimal altitude and velocity to minimize fuel consumption.

- *Phase 5: Release Manoeuvre*
  The *release manoeuvre* (Figure 1e) involves release of the RLV by the TA close to the runway. The RLV lands horizontally onto the landing strip using its own landing gear.

This paper builds on the previously presented modelling and dynamics of *capture phase* of IAC presented in [6] and [7]. The goal of this phase is to establish contact with the RLV within 70 s of *formation flight* and connect the TA and RLV with a rope. This manoeuvre requires a high degree of agility and accuracy to allow for multiple capture attempts. For this, the capturing device must overcome external disturbances from the flexible rope and the wake of the aircraft. In Section 2, a brief overview of the capturing device and the associated environment is presented. The rope properties themselves are critical to the dynamics and therefore, sensitivity to factors like length, diameter and other properties, are investigated through open-loop tests. Section 2 also includes a suitable control approach for the *capture phase* to allow manoeuvrability in the presence of rope vibrations. A robust control architecture with active damping is proposed. Then, in Section 3, open loop tests are performed to check the stability of the system and strength of the chosen rope. Closed loop simulations are also performed to analyse if the capturing device can perform multiple manoeuvres within the capture window. The final conclusions and future work are summarized in Section 4.

2. Modelling and Dynamics of Capture Phase

This section summarises critical aspects of modelling the *capture phase*. First, the selected design for the capturing device along with its basic operating principle is presented. Then, the major disturbing factors that could affect the dynamics of the system, like wake from the TA and vibrations from the rope are introduced. Lastly, a robust control approach is proposed such that the capturing device can perform multiple manoeuvres even in the presence of perturbations.

2.1 Aerodynamically Controlled Capturing Device (ACCD)

From previous studies, the most promising capturing technique was found to be an Aerodynamically Controlled Capturing Device (ACCD) [9]. This device showed the best performance and agility, while posing the lowest risk. Figure 2 shows a schematic of the ACCD. It is 2 m long with a cross-sectional diameter of 1.5 m including the fins. The four flaps, which can deflect up to a maximum of ±15° provide 6DOF agility and control. The nose of the ACCD is attached to the TA via rope and the capturing mechanism at the back of the ACCD secures the connection with the RLV (using a lock-in mechanism with a boom on RLV).

Figure 3 shows how roll, pitch and yaw deflections are realized using the four flaps. For pitch, both horizontal flaps deflect in the same direction. For yaw, both the vertical flaps are deflected in the same direction. And for roll, all flaps are deflected. These symmetric configurations of flap deflections up to 10° for pitch, yaw and roll motion were simulated using Reynolds Averaged Navier-Stokes (RANS) computations for the range of ±15° angle of attack to get a better understanding of its aerodynamic performance and stability characteristics. This data is further used in the dynamic simulations of the *capture phase*. The simulation specifications and detailed analysis of the aerodynamic characteristics can be found in [6] and [7].

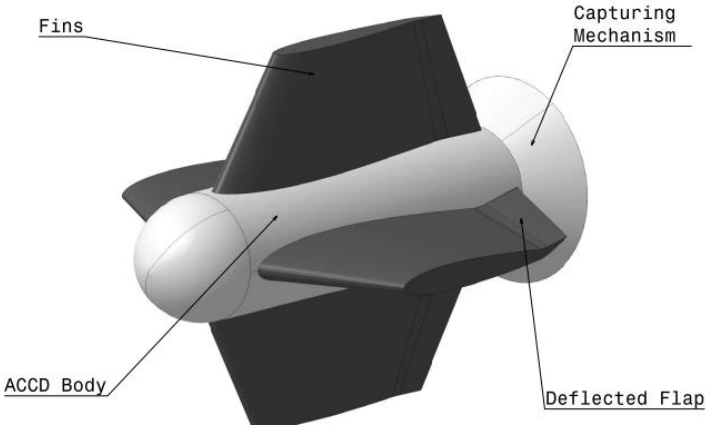

Figure 2: ACCD Geometry with Four Symmetric Fins

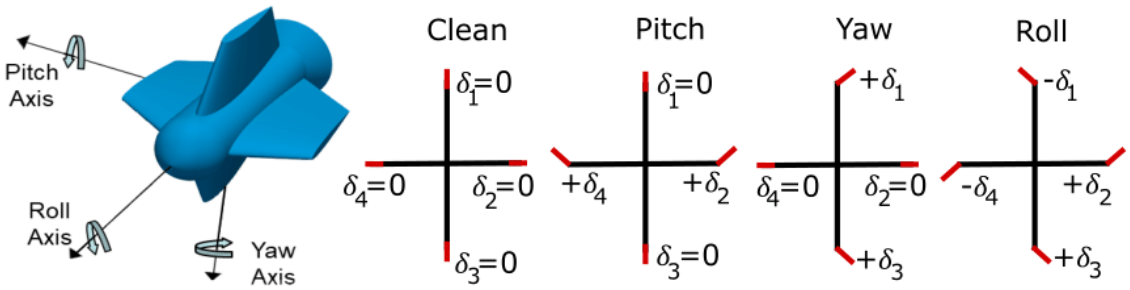

Figure 3: Conventions for ACCD Flap Deflections and Resulting Moments

2.2 Aircraft Wake

Based on a detailed study of aircraft wake documented in [5] and [6], it was established that the aircraft wake has a significant downwash (vertical) component at higher angles of attack. Figure 4 shows the velocity contour of the wake trailing behind the TA, generated using RANS. It is clear from the figure that the change in velocity due to the wake is evident even at a distance of 315 m from the aircraft nose. Since the ACCD is required to trail behind the aircraft during the *capture phase*, the exposure to wake is very likely. Additionally, the aircraft is expected to have high angles of attack during the *formation flight*, thereby exposing the ACCD to very large disturbances. Thus, it is critical to analyse these effects in controlled flight simulations of the ACCD.

Figure 5 shows the wake velocity profiles in the fuselage plane as a fraction of free-stream velocity (U_∞). The distance from the aircraft along horizontal (y) and vertical (z) directions are scaled using aircraft length ($L \approx 70$ m). It can be observed that, the streamwise (horizontal) velocity component reduces with the distance from TA and is limited to a width of z/L = ±0.25. However, the downwash (vertical) velocity component does not fade away even with increasing distance from the aircraft and spans a width over z/L = ±0.50 from the nose of the aircraft. For an angle of attack of 6°, this component (U_z) was found to reach about 8% of free stream velocity even at a distance of 315 m from the aircraft. This can pose a major challenge in the control of ACCD, as the device experiences continuously changing velocity as well as turbulence. This could lead to disturbances in its angle of attack, which in turn affects the pitch manoeuvres.

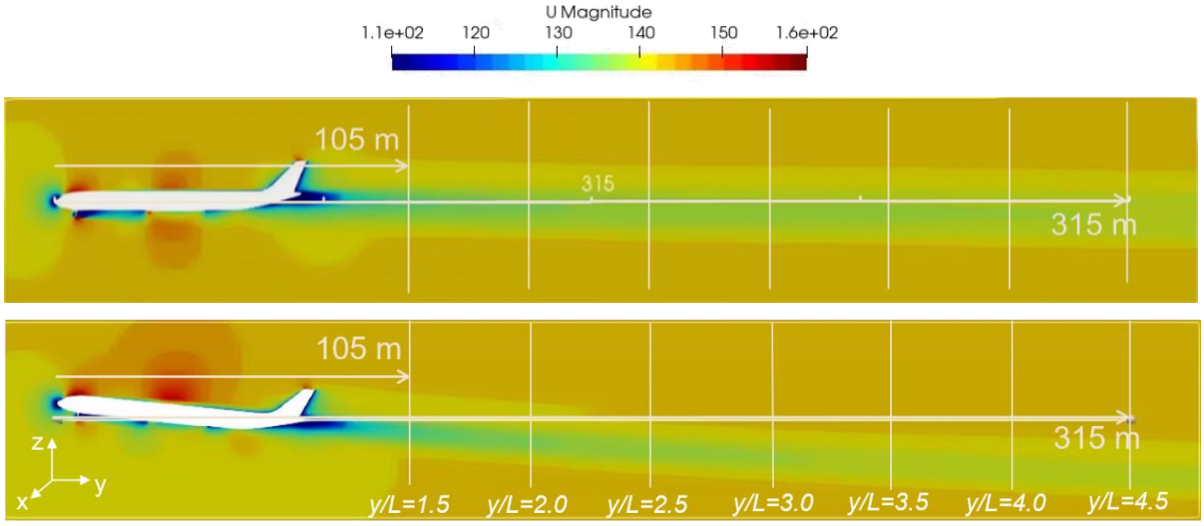

Figure 4: Velocity Magnitude Contours for Angle of Attack of 0° (top) and 6° (bottom)

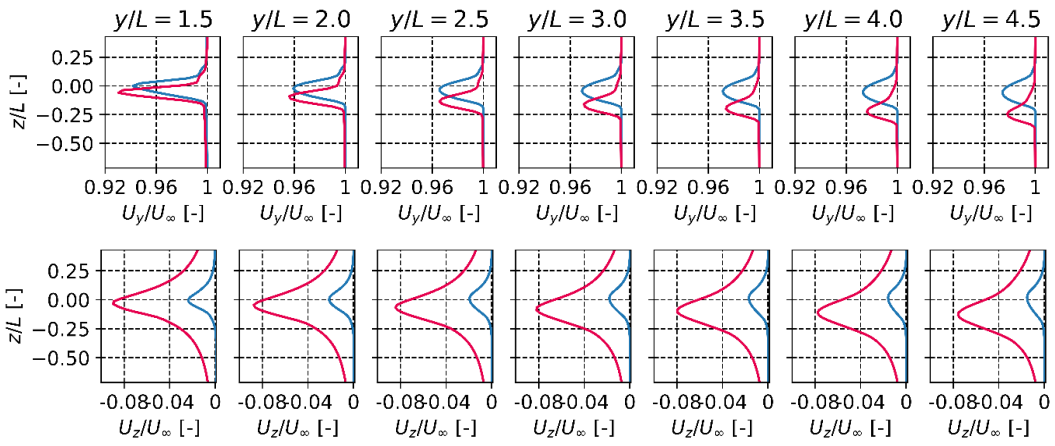

Figure 5:Wake Profiles in the Fuselage Plane for 0° (blue) and 6° (red) Angle of Attack; Streamwise Velocity Component (top) and Downwash Velocity Component (bottom)

2.3 Flexible Rope Model

An important aspect of *capture phase* is the design, modelling, and simulation of the towing rope dynamics. Based on the ACCD dynamics, the towing rope and the vehicle trajectories, a multibody simulation is set up. The towing rope is modelled as a chain of *n* rigid bodies of length *l*, connected with spring-damper elements in order to approximate the flexible dynamics [10]. Each body (rope segment) has a mass of *m* such that the total rope mass is the sum of the mass of each segment. This can be visualized in Figure 6. The deformation of these discrete rigid elements creates a curvature, such that the behaviour of a flexible body is captured as shown in Figure 7. The bending stiffness is modelled with identical springs of stiffness *K* placed at each joint of the rope segment. To capture the aerodynamics of the rope, a drag model based on [12] is also included. Further modelling details of the rope can be found in [6].

For the rope model, the chosen material is a high strength fibre rope featuring extremely low stretch consisting of UHMWPE (Ultra-High-Molecular-Weight Polyethylene) fibres. The optimized rope design and an extremely compact and stable rope structure serves as a good fit for IAC. The main advantage of choosing this model is that it permits a one-to-one substitution of a steel wire rope at the same diameter without the need for converting or adapting the periphery - at only 1/7 of the weight [13]. The ropes are therefore known to be lightweight and also offer vibration damping attributes. They are widely used in marine, sports, medical and space applications [14].

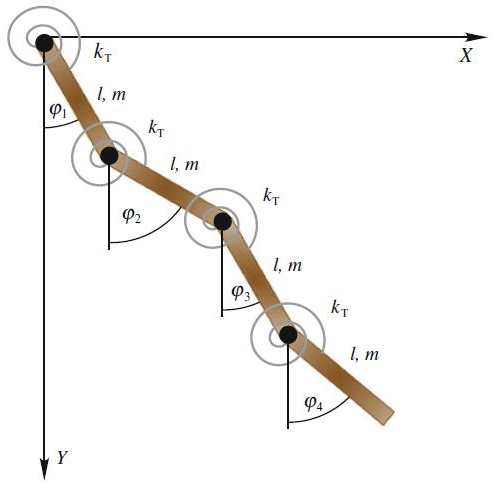

Figure 6: Discrete Rope Model with Elastic Joints [11]

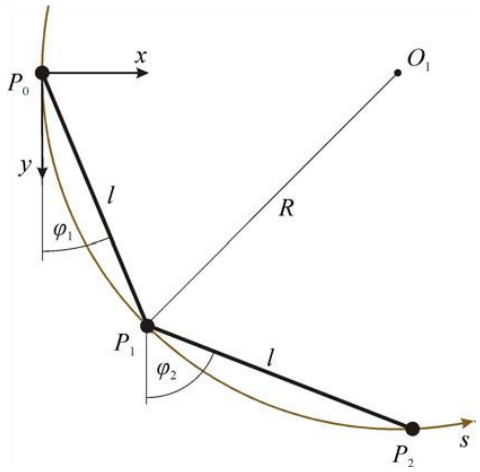

Figure 7: Radius of Curvature Between Two Segments [11]

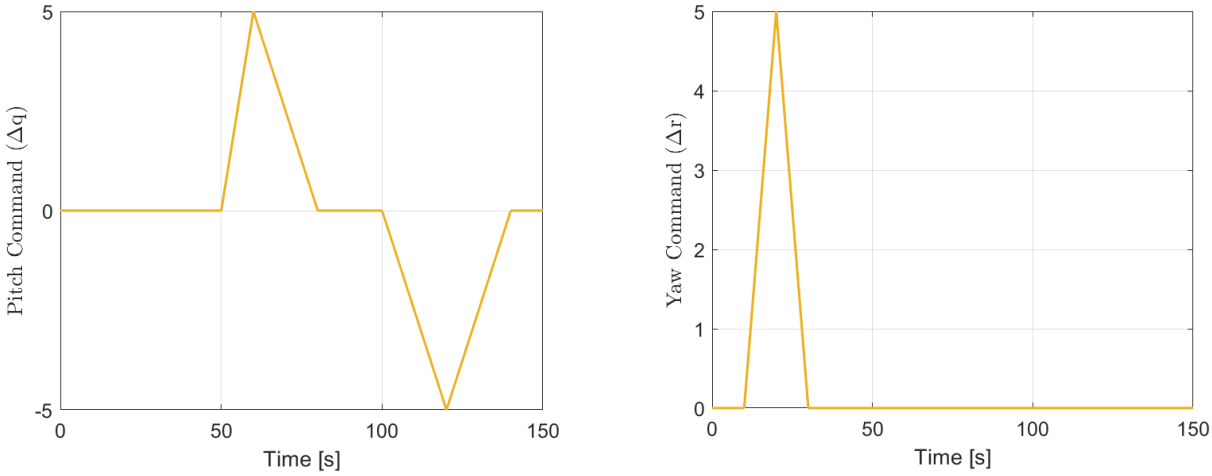

Figure 8: Test Control Commands in Pitch Direction (left) and Yaw Direction (Right)

An integral part of the dynamics of the system also comes from the properties of the rope. These include aspects like length, diameter, weight and so on. To ensure adequate manoeuvrability of the ACCD, the rope must be lightweight. However, the rope should also be strong enough to withstand the towing forces after the *capture phase*, when the RLV is already attached. Another important factor that must be analysed is the effect of discretisation. The higher the discretisation, the closer rope behaves to reality. However, computationally it is not viable to include very large number of discretised elements and there needs to be a trade-off between accuracy and computation time. Thus, a sensitivity study is performed to analyse the most suitable configuration of the rope. For the dynamic simulations, it is assumed that one end of the rope is connected to the aircraft while the other end of the rope is attached to the ACCD. A simple set of control commands in pitch and yaw direction (shown in Figure 8) are used to check the manoeuvrability of the ACCD. The system is commanded to pitch up and down by 5° each and also, a yaw angle of 5° is commanded. The ACCD realises these commands by deflecting its flaps as described in Section 2.1.

2.3.1 Sensitivity to Rope Diameter

Some rope characteristics for a rope of 150 m with two different diameters (16 mm and 32 mm) are summarised in Table 1. It can be observed from the table that by doubling the diameter, the rope becomes heavier by almost four times. Further, the bending and axial stiffness also increases substantially, which results in a rather stiff rope. On one hand a stiffer rope could lower the amplitude of vibrations coming from the rope, while on the other, this can considerably reduce the manoeuvrability of the ACCD. Hence, an open loop test is performed using basic commands shown in Figure 8 to check the manoeuvrability and stability of the system.

Table 1: Rope Characteristics for a 150 m Rope with Different Diameters

Rope Property	**16 mm**	**32 mm**
Young's Modulus [GPa]	87	87
Damping Coefficient [-]	0.07	0.07
Mass [kg]	23.40	83.25
Area Moment of Inertia [m^4]	3.2161×10^{-9}	5.1471×10^{-8}
Polar Moment of Inertia [m^4]	6.4339×10^{-9}	1.0294×10^{-7}
Bending Stiffness [Nm/rad]	55.9756	895.6103
Bending Damping [Nms/rad]	5.9421×10^{-5}	9.5054×10^{-4}
Axial Stiffness [N/m]	1.1662×10^{5}	4.6646×10^{5}
Axial Damping [Ns/m]	42.2235	159.2826

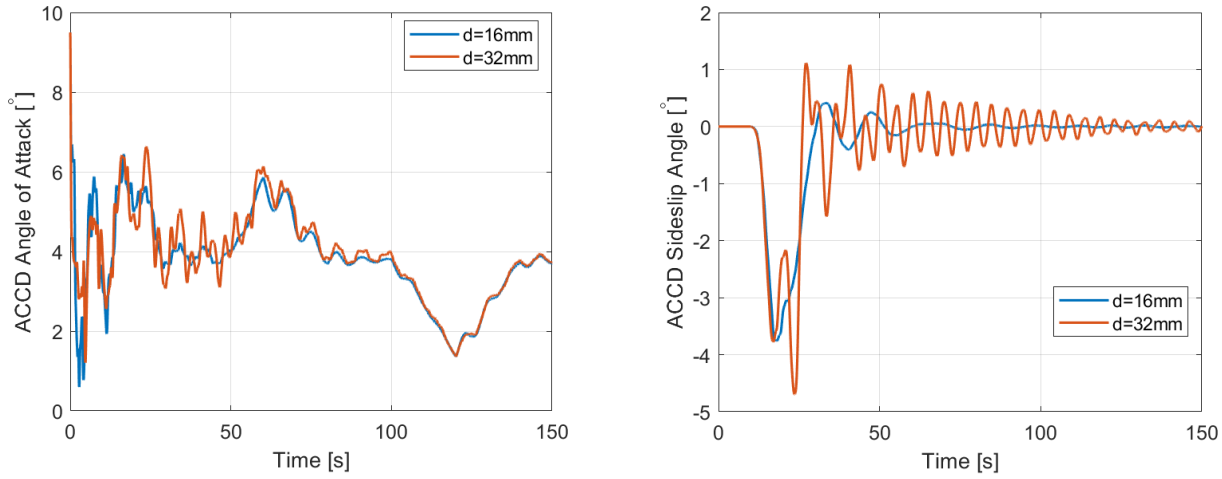

Figure 9: Effect of Diameter on Aerodynamic Angles of ACCD: Angle of Attack (Left) and Sideslip Angle (Right)

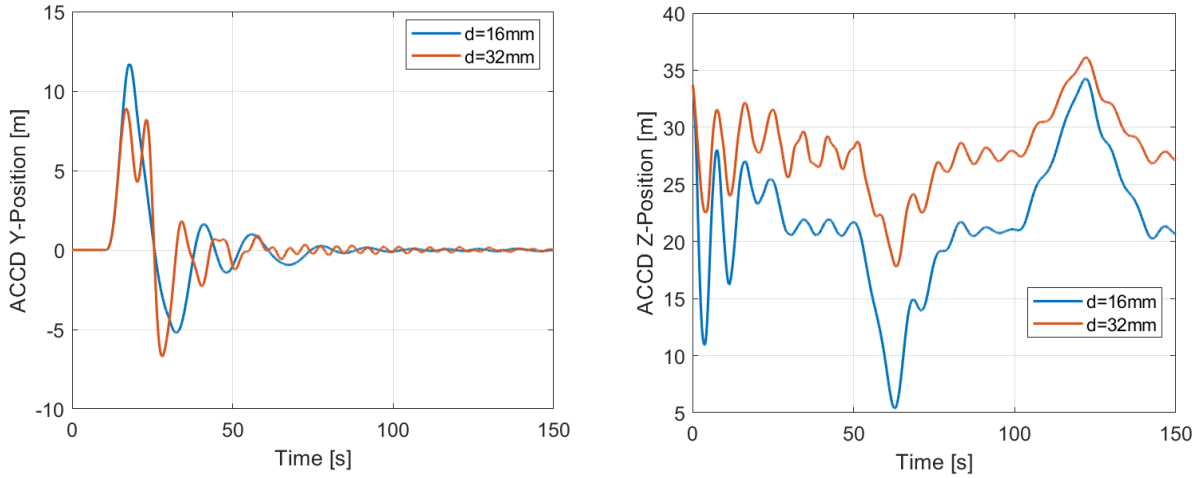

Figure 10: Effect of Diameter on Position of ACCD in Lateral (Y-Position) and Vertical (Z-Position) Direction

Figure 9 shows the effect of diameter on the angle of attack and sideslip angle of ACCD. It can be observed from the plots that vibrations appear to be more evident when a rope diameter of 32 mm is used. As a result, the vibrations also take longer time to dampen out and the system needs longer to stabilize. This can be attributed to the fact that a thicker diameter results in a stiffer rope. Stiffer systems typically tend to increase the natural frequency of the system [15]. Additionally, very stiff systems can result in numerical instabilities. Figure 10 shows the effect of diameter on the position of ACCD in the lateral and vertical directions. For the same command in pitch direction (Figure 8), it appears that the ACCD moves about 15 m for a 16 mm diameter rope in vertical direction, while it is only able to move 10 m for the 32 mm diameter rope (Note: Sign convention for Z-direction is positive downwards). Similar observation can also be made in the lateral direction, wherein the ACCD is more mobile for the 16 mm diameter. This confirms the claim that the heavier rope reduces the manoeuvrability of ACCD. Since it is favourable to have a highly agile system which can be stabilized quickly, the rope model with 16 mm diameter is considered a better fit.

2.3.2 Sensitivity to Rope Length

Rope length is another property that can affect the dynamics of the system. A short rope could have a limited range in terms of manoeuvrability. On the other hand, longer ropes are heavier and may have larger vibrations that require more time to dampen out. Longer ropes can also require larger rope discretisation for the dynamics to be adequately represented. This results in increased computational effort. An open loop test is performed with different rope lengths using the commands shown in Figure 8 with rope diameter of 16 mm and 30 rope segments.

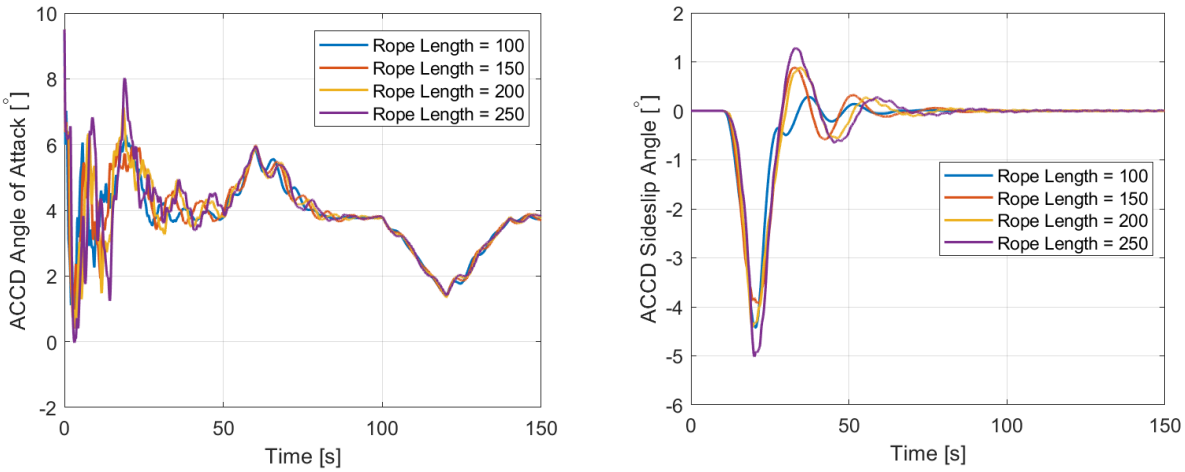

Figure 11: Effect of Length on Aerodynamic Angles of ACCD: Angle of Attack (Left) and Sideslip Angle (Right)

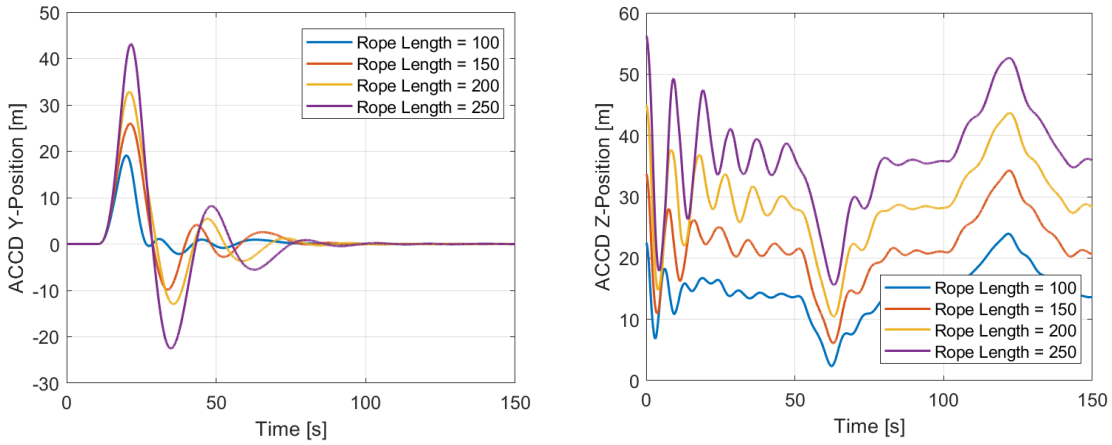

Figure 12: Effect of Length on Position of ACCD in Lateral (Y-Position) and Vertical (Z-Position) Direction

It can be observed from Figure 11 and Figure 12 that the longer rope of 250 m results in a larger movement than the shorter ropes. However, the rope also shows larger amplitude in vibrations and requires longer settling times. For larger control commands, the amplitude could become even larger. This could counteract the manoeuvrability of the system by requiring longer settling times, thereby making it difficult for the system to perform multiple corrective manoeuvres during the capture of RLV. On analysing the displacement in vertical direction (Figure 12 right), it can be observed that, the heavier and longer ropes tend to stabilize at a lower position in the Z-direction (about 35 m below the reference for 250 m). This could be advantageous when it comes to exposure to wake because the shorter ropes stabilize very close to the wake. Thus, the possibility of using a longer rope should not be overlooked. Nonetheless, due to the benefit of lower computation effort and faster settling times, an intermediate rope of length 150 m is selected. This can be reiterated when tested with wake.

2.3.3 Sensitivity to Rope Discretisation

Since the rope is modelled as a chain of elements, a larger discretisation should result in a response that is closer to a flexible rope. But an increased discretisation requires more computation effort. Thus, it is worthwhile to find a balance between accuracy and computation time. Open loop tests are performed with a rope of 16 mm diameter and 150 m length, discretised into 10, 20 and 30 segments respectively, using control commands shown in Figure 8. Figure 13 show the pitch angle displacement of first and last node of the rope. It can be observed that the displacement of these angles due to different rope segments are distinct. But the magnitude of displacement remains comparable. This is because of the large torsional damping factors considered at the attachment of rope-aircraft and ACCD-rope (as stated in [6]). Nonetheless, a discretisation of 30 segments is considered to be able to appropriately represent the dynamics. A less refined model of 10 segments is used for controller tuning applications since the response is comparable. Based on the sensitivity study, a final rope model with diameter 16 mm, length 150 m and discretisation of 30 segments is considered for the closed loop tests.

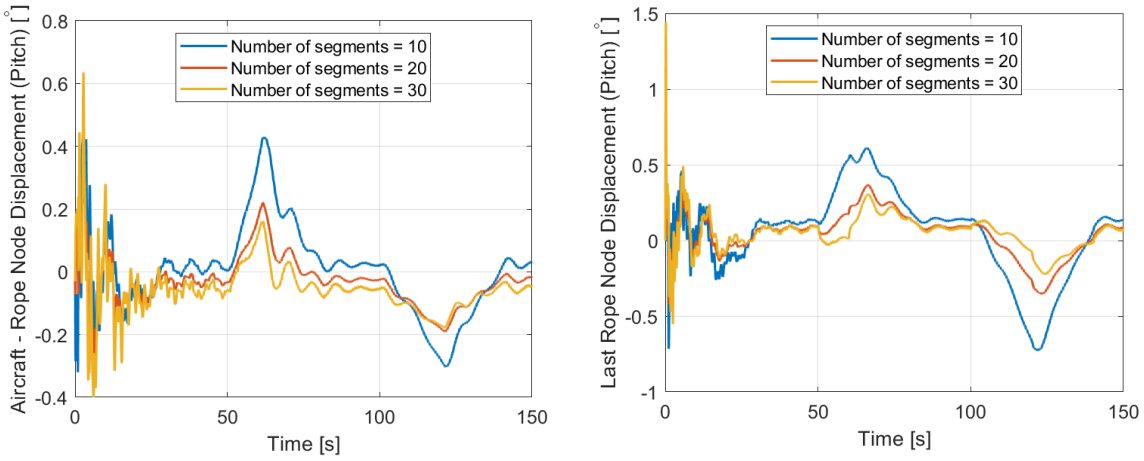

Figure 13: Effect of Discretisation on Pitch Angle of ACCD: First Node (Left) and Last Node (Right)

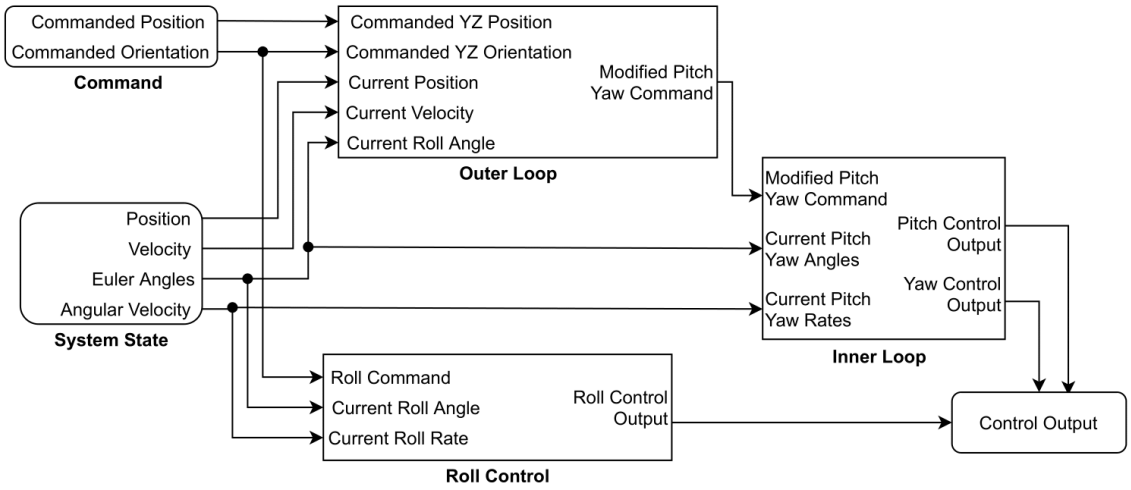

Figure 14: Control Architecture for ACCD during Capture Phase

2.4 Control Design

The capture window for the ACCD during which the RLV and the TA remain in formation, is estimated to be about 70 s [5]. During this period, the ACCD should be able to perform multiple capture attempts if required. Thus, for effective control of ACCD, the controller should drive the device to the commanded state of RLV in the presence of external disturbances within a short time. This is to be achieved using the four aerodynamic surfaces, as shown in Figure 3. A control architecture was previously proposed in [6] based on these requirements. The proposed controller is shown in Figure 14. Since ACCD is axisymmetric, a change in roll orientation can lead to a motion in a completely different direction, when the fins are deflected. Thus, a roll rate damper is included to maintain a steady orientation. The pitch and yaw control are performed in two loops. The outer loop translates the commanded YZ position and orientation into a modified command (angular displacement) based on the roll orientation of the system. The inner loop then uses these modified commands to generate the required control moment for the manoeuvre. Hence, the overall concept is based on Cascaded PD Control.

An important iteration that was identified for the control design in [6], is the need for active damping. Although the rope includes internal structural damping which helps the system stabilize over a period of time, it can take minutes for the vibrations to completely dampen out. This can be observed in the sensitivity analysis performed in Section 2.3 (for instance, Figure 11). With such long period vibrations, it becomes infeasible to perform multiple corrective manoeuvres within a span of 70 s of capture window. Further, applying control commands when ACCD is still oscillating can destabilize the system and lead to capture failure. Thus, it is essential to include an aspect of vibration control in the control design.

2.4.1 Active Damping

In order to actively control the rope dynamics, the characteristics of the vibrations must be closely analysed. Using a response from a simple open loop signal (for example, Figure 11 and Figure 12), Fourier transform can be used to determine the natural frequencies present in the signal. Here, the major disturbing frequencies can be identified based on the amplitude spectrum (which frequencies have higher amplitudes). The low frequency vibrations can often be corrected as a part of the dynamics. However, while correcting for the higher frequency vibrations, the controller can end up amplifying the disturbances, leading to limit cycle behavior and destabilizing the system. Thus, it is a common practice in control design to reject such frequencies from the main input signal to the controller.

To remove unwanted components from a signal, filters are typically used. The filters are often used in combination with PD, PI or PID controllers to generate robust feedback controllers. For the current application, a low-pass filter is considered fitting [16]. A low pass filter is used to pass signals with frequency lower than a certain cut-off frequency. In other words, all frequencies lower than the specified value are allowed to pass, while any frequencies higher than the cut-off frequency are blocked by the filter (allowing them to dampen out naturally). It must be mentioned that filters often end up introducing a phase shift in the input signal, leading to an output that shifts in time. Signals are typically restored back to the original form using lead-lag compensators [16]. However, for the current application, the phase of the vibrations can be considered

irrelevant and the main focus is on the damping of the vibrations that act as a disturbance to the system. Therefore, there is no requirement to regulate the phase of the vibrations. A simple first-order filter can be realised using the following transfer function:

$$H(s) = K.\frac{\omega_{lp}}{s + \omega_{lp}} \tag{1}$$

Here, K denotes the gain and ω_{lp} denotes the cut-off angular frequency in rad/s.

Using the low-pass filters in combination with the Cascaded PD controller, a robust controller for closed-loop simulation of *capture phase* can be tested. Figure 15 shows the response of the system with and without active damping. It can be observed that the settling time without active damping is about 50 s, while with active damping, the vibrations are able to dampen out in approximately 15 s. The amplitude of vibrations also appears to have reduced as a result of active damping. This would allow the ACCD to make multiple manoeuvres as the vibrations dampen out much quicker, creating a more stable system. In the next section, closed-loop simulations will be analysed using this controller.

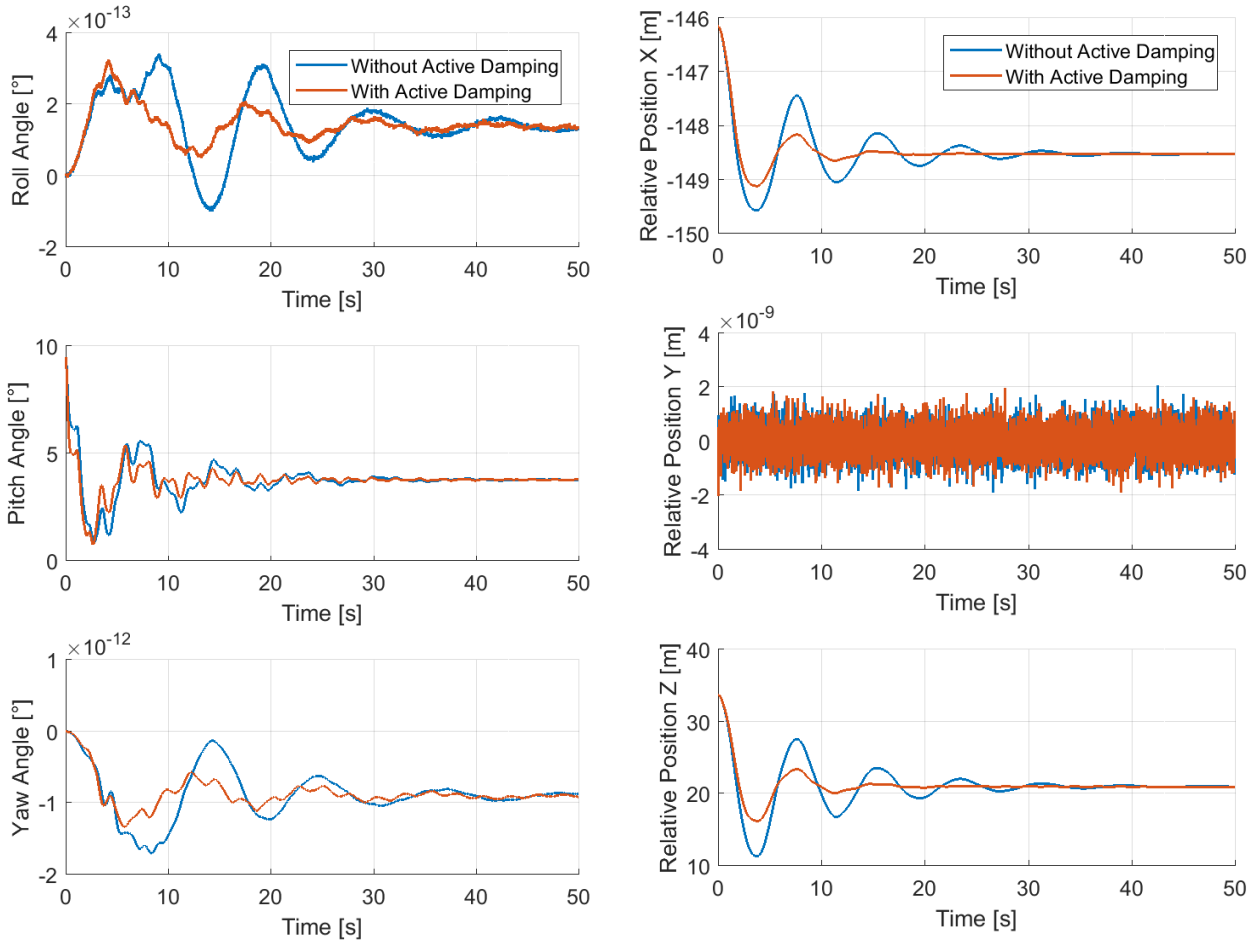

a) Effect of Active Damping on ACCD Body Angles

b) Effect of Active Damping on ACCD Position

Figure 15: Effect of Active Damping on Stability of ACCD

3. Results

The complete simulation model for *capture phase* of IAC [6], can now be used to check the suitability of the chosen rope properties in Section 2. Before the capture process begins, the ACCD is first released from TA. During the deployment process, the system (rope + ACCD) should remain stable even in the presence of the aircraft wake. Since it was already established in [6] that ACCD is statically stable, the test will provide an outlook on the stability of the rope model with the chosen properties. Additionally, the rope should also be strong enough to support the towing loads from the RLV without reaching its breaking limit. Therefore, tests are performed in open loop (without control) to check these critical aspects of the rope.

The robust control design proposed in Section 2, will also be tested through closed-loop simulations. These simulations are performed keeping in mind that the ACCD should be able to execute multiple manoeuvres within the capture window of approximately 70 s. The results are presented with and without the wake to analyse if the ACCD can effectively manoeuvre in both environments. Any additional iterations are proposed based on the response of the system.

3.1 Open Loop Simulations

The open loop simulations are performed at cruise conditions with the TA flying at an altitude of 6000 m with a velocity of 142.39 m/s (Ma = 0.45). The rope is assumed to have a diameter of 16 mm discretised into 30 segments, and is tested up to a maximum length of 250 m. Through these tests, one of the goals is to check the stability of the system when the ACCD is being deployed from the aircraft. Another critical aspect is to study the effect of wake when ACCD is uncontrolled to form as a baseline for controlled simulations. Lastly, the selected rope model must be tested to check if it can withstand the maximum towing loads without breaking.

3.1.1 Rope Deployment

This simulation shows the rope being deployed at the rate of 2.5 m/s to its maximum length of 250 m. This test is performed with and without wake to analyse its effects without control. While the rope is being deployed, the effect of wake is most evident in the vertical direction. Figure 16 and Figure 17 show the effect of wake on the pitch orientation and vertical displacement of ACCD respectively. It can be noticed that the effect of the wake is larger while the rope is shorter. This is expected since the ACCD with a smaller rope is closer to the wake, and as the rope is deployed it moves further down in the Z-direction due to its mass, away from the dominant parts of the wake. It also appears that the wake introduces a drift in the Z-displacement of ACCD. This is likely because the ACCD experiences lower velocities than the typical free stream, resulting in different pitch stability characteristics. Nonetheless, the multibody rope model remained stable throughout the simulated deployment process.

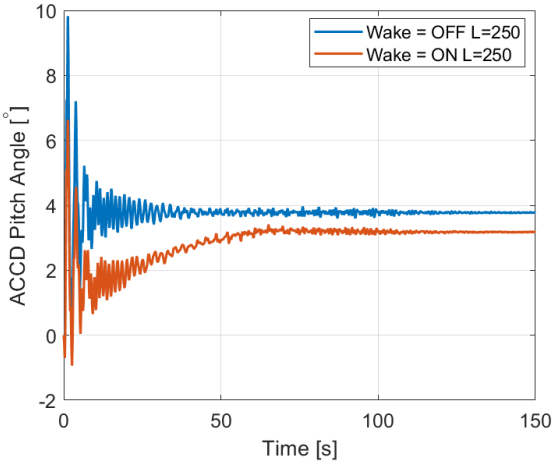

Figure 16: Effect of Wake on Pitch Angle of ACCD

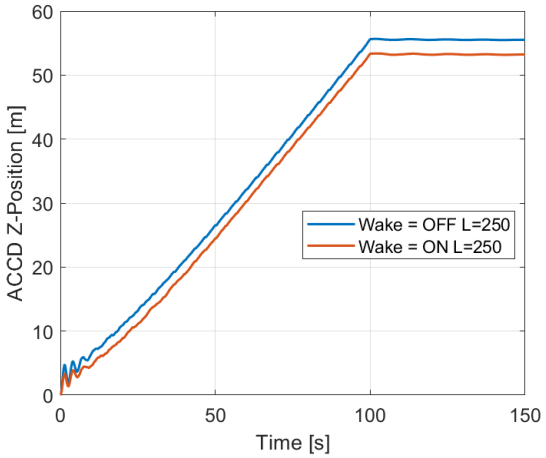

Figure 17: Effect of Wake on Vertical Position of ACCD

3.1.2 Maximum Elongation in Rope

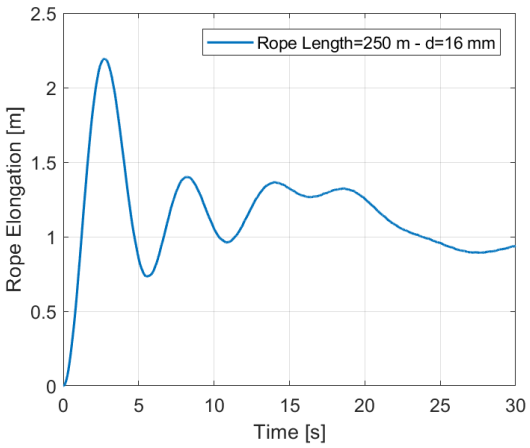

Figure 18: Elongation of Rope due to Towing Loads

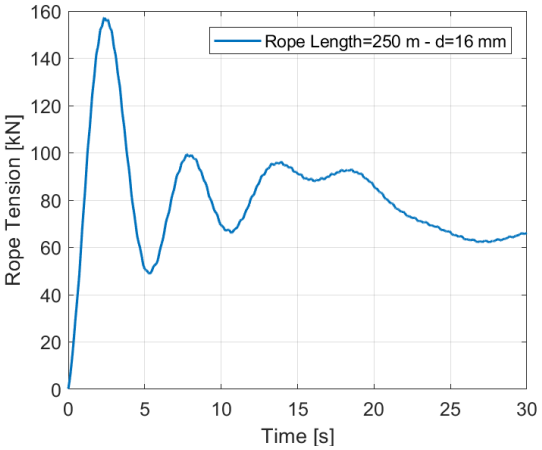

Figure 19: Tension in Rope due to Towing Loads

This test case is a simplified simulation to check if the rope is capable to withstand the maximum possible tension after the RLV has been captured and is being towed. Full-scale test cases, as proposed in [5] are used for the current simulation. The TA is assumed to be the long-range jetliner A340-600 with four engines. Each engine is expected to deliver up to 260 kN of thrust at sea level. The RLV on the other hand is the first stage of a 3-Stage-To-Orbit concept, weighing approximately 80 tons. Further detail on the test cases can be found in [5]. To consider the worst-case scenario in terms of maximum rope tension, the aircraft is assumed to be at maximum thrust in its minimum drag configuration. The RLV is then assumed to generate maximum drag. Looking into the maximum tension of the rope (Figure 19), it can be observed that it is around 155 kN, which is about 55% of the minimum breaking strength of the rope model at 16 mm diameter [13]. Also, the maximum rope elongation (Figure 18) is around 2 m, which is less than 1% of the total length, while the selected rope design is rated for a maximum of 3.5% elongation [13].

3.2 Closed Loop Simulations

In the previous section, it was established that the rope is fitting for the purpose of IAC and the system could stabilize even without control. In this section, closed-loop tests with multiple manoeuvres are presented to examine the agility and stability of the system. The ACCD is controlled using the robust controller shown in Section 2.4. The simulation starts when a rope of diameter 16 mm is deployed to a length of 150 m (as previously selected in Section 2.3). Once the deployment is completed, the controller is immediately turned on to help with the active damping of the vibrations. During a span of 80 s, multiple manoeuvres are attempted in both Y- and Z- directions. The test is then repeated in the presence of wake to check if the controller can achieve its target in the presence of strong disturbances.

3.2.1 Ramp Response

Figure 20 and Figure 21 show the response of ACCD in close-loop. The ramp command signal directs the ACCD to move 10 m (closer to the wake) above its stability point at approximately 20 m in the vertical direction. Then at 40 s, it is commanded to return to its original position. Meanwhile, in the lateral direction, it is commanded to move 5 m to the left and at 40 s, move to the opposite direction spanning about 11 m. From the figures, it can be observed that the ACCD is able to achieve the commanded motion spanning over 10 m in both directions within 65 s (considering first 15 s for damping of initial vibrations. Further, it can be observed that a small roll angle is introduced during the manoeuvres. This is quickly dampened out using the roll controller, avoiding any drift in Y- or Z- directions. It must also be mentioned that the flap deflections remain unsaturated, which suggests that there is further room for manoeuvrability. To conclude, ACCD is able to perform multiple manoeuvres of up to 10 m in both Y- and Z- directions, even with the vibrations coming from the rope.

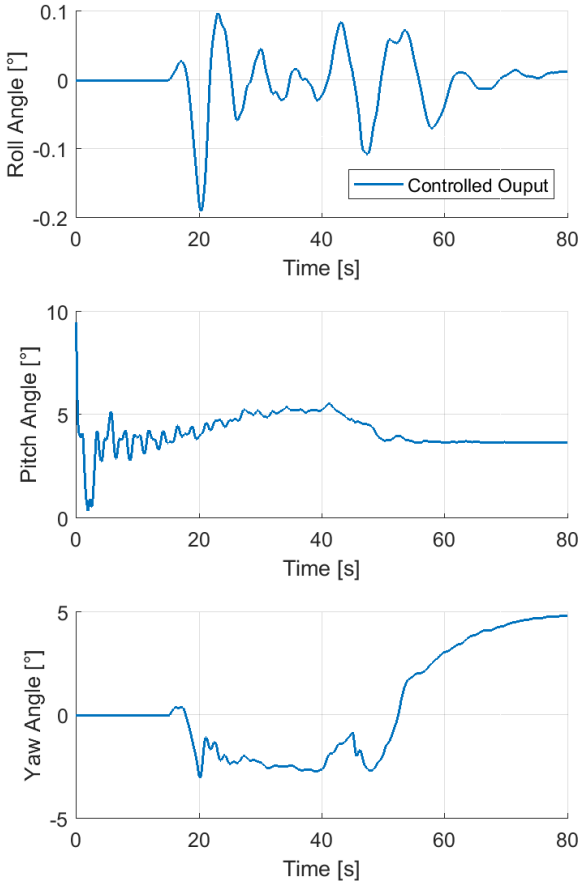

Figure 20: Controlled Response of ACCD Angles

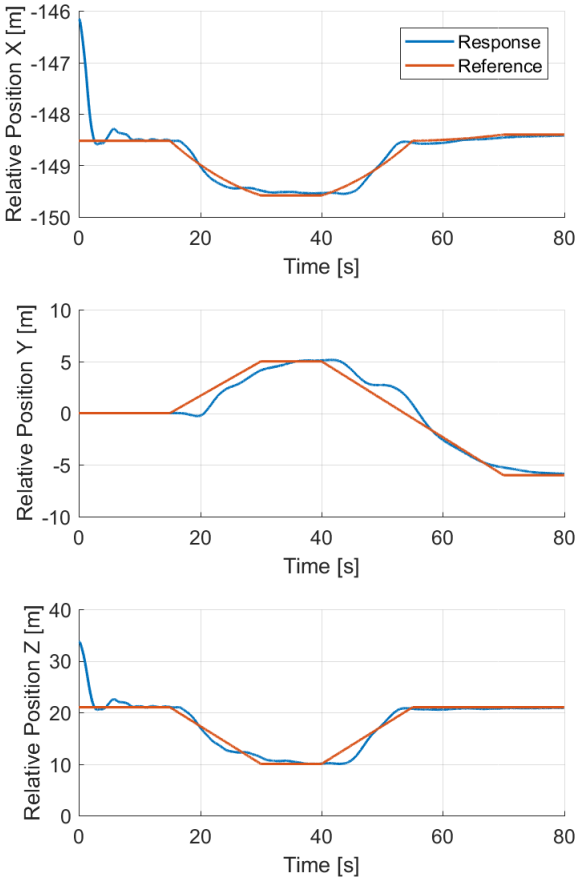

Figure 21: Controlled Response of ACCD Position

3.2.2 Effect of Wake

Using the same command, the simulation is now performed with the wake included. Figure 22 and Figure 23 show the response of the system in closed-loop. The first observation that can be made, is the offset in the position (mainly seen in X- and Z- direction). This is because the ACCD sees a reduced free stream velocity because of the wake and hence, responds differently. A similar observation was also made in the open loop tests shown in Figure 16 and Figure 17. When the command is to move up by 10 m in the pitch direction, the ACCD shows unstable behaviour. This is expected, since the ACCD moves closer to the wake, where the disturbances are very strong. The disturbances are also evident in the Y-direction when the ACCD is close to the wake. In conclusion, the ACCD is unable to manoeuvre when it is too close to the wake. It is possible for ACCD to manoeuvre in the opposite direction away from the wake, but this would leave the ACCD with only half of the range in Z-direction for the capture. Thus, alternative solutions need to be considered.

One possible solution is to consider a longer rope. It was established in the sensitivity study shown in Figure 12, that longer ropes stabilize lower in the Z-direction due to the extra weight. A rope of length 150 m stabilizes 20 m below the reference line (aircraft nose), while a rope of 250 m stabilizes at a little over 35 m. This keeps the ACCD outside the most perturbing regions of the wake, allowing it to maneouvre a larger range in the Z-direction. This approach can be further confirmed by Figure 24, which shows the turbulent kinetic energy experienced by ropes of different lengths, while performing simple maneouvres shown in Figure 8. A higher value of turbulent kinetic energy can be linked to when the system experiences the largest turbulence due to wake. It can be observed that the rope of 250 m experiences the least turbulence while performing the same maneouvre.

Since the effects of wake can be seen as far as 35 m in the Z-direction (see Figure 5), some additional control iterations may be required to correct for the continuously changing velocities. The change in velocity introduces offsets in the control response, and the ACCD fails to meet the commanded value accurately. An improved control design for such an evolving environment can be achieved through gain scheduling at different velocities. This will allow the control gains to evolve with the changing airspeed and potentially provide more effective control.

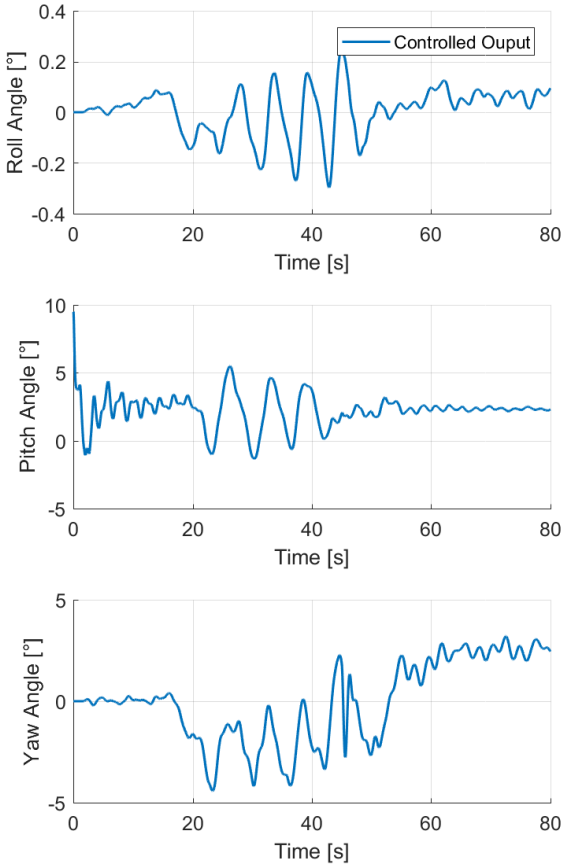

Figure 22: Effect of Wake on ACCD Angles (Closed-Loop)

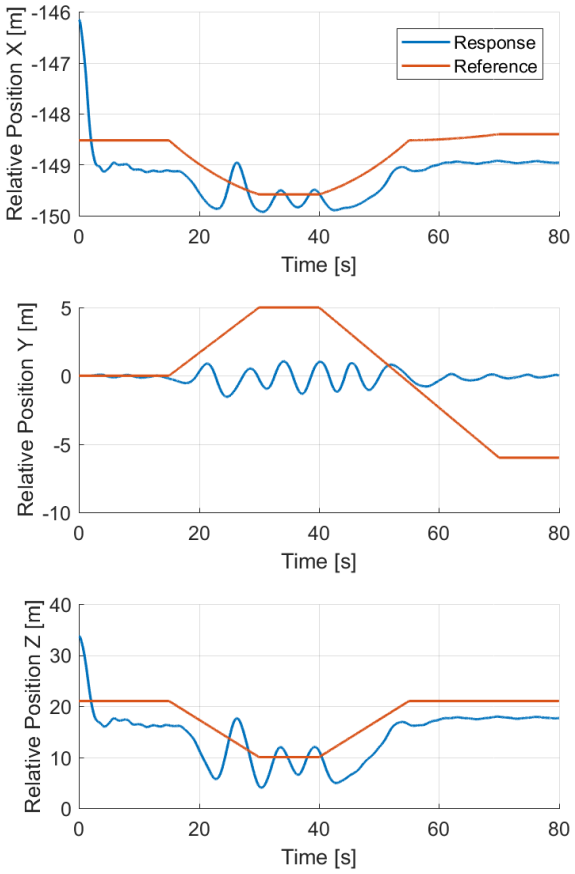

Figure 23: Effect of Wake on ACCD Position (Closed-Loop)

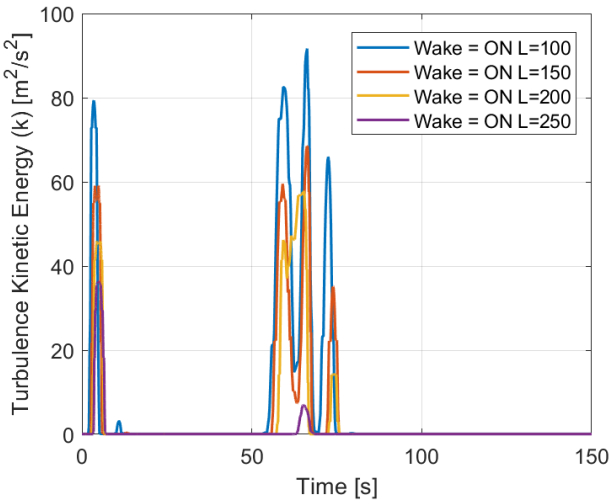

Figure 24: Turbulence Kinetic Energy for Ropes with Different Length

4. Conclusions and Future Work

The paper investigates the *capture phase* of IAC. During this phase, ACCD attached via rope to the TA, navigates its way to the RLV to establish contact. The capture takes place when the TA and RLV are in a parallel formation flight. The current study is focussed on the rope dynamics, and control of the ACCD attached to it. Through an extensive sensitivity analysis of the properties, a rope with 16 mm diameter and 150 m length was chosen. On testing the rope for stability during deployment (through open loop simulations), it was established that the rope remained stable even in the presence of wake. Further, the rope strength was checked by simulation of maximum towing loads during IAC. It was confirmed that the maximum tension and elongation of the rope is well within its design limits, making it suitable for IAC.

A robust control architecture with active damping was proposed as a part of this study. Closed-loop simulations showed that the vibrations damped out much faster (approximately by 35 s) when compared to the simulations where no control was used. Additionally, ACCD was able to perform multiple maneouvres in both vertical and horizontal directions within a period of 65 s, when no wake was considered. However, when the disturbances from the wake were included, the ACCD destabilized in regions close to the most dominant parts of wake. This problem can be mitigated by use of a longer rope (250 m), which stabilizes lower in Z-direction, away from the wake. Future iterations of the controller could also include gain scheduling, which would help deal with the issue of continuously changing airspeed in the wake.

Acknowledgements

This work was performed under the Horizon 2020 project '**F**ormation flight for in-**A**ir **L**auncher 1st stage **C**apturing demonstrati**on**' (**FALCon**) aimed at development and testing of the "In-Air Capturing" technology. FALCon, coordinated by DLR-SART, is supported by the EU within the Programme 5.iii. Leadership in Enabling and Industrial Technologies – Space with EC grant 821953. Further information on FALCon can be found at http://www.FALCon-iac.eu

List of Abbreviations

Abbreviation	Definition
ACCD	Aerodynamically Controlled Capturing Device
CFD	Computational Fluid Dynamics
DLR	German Aerospace Center
IAC	In-Air Capturing
L/D	Lift-to-Drag
MECO	Main Engine Cut Off
PID	Proportional Integrator Derivative
RANS	Reynolds-Averaged Naviers Stokes
RLV	Reusable Launch Vehicle
TA	Towing Aircraft
VTHL	Vertical Take-Off Horizontal Landing
VTVL	Vertical Take-Off Vertical Landing

References

[1] Patentschrift (patent specification) DE 101 47 144 C1, Verfahren zum Bergen einer Stufe eines mehr-stufigen Raumtransportsystems, released 2003.

[2] M. Sippel, J. Klevanski, J. Kauffmann, "Innovative Method for Return to the Launch Site of Reusable Winged Stages," IAF-01-V.3.08, *52nd International Astronautical Congress*, 2001.

[3] S. Stappert, J. Wilken, L. Bussler, M. Sippel, "A Systematic Assessment and Comparison of Reusable First Stage Return Options", IAC-19-D2.3.10, *70th International Astronautical Congress*, 2019.

[4] M. Sippel, S. Stappert, S. Singh, "RLV-Return Mode "In-Air-Capturing" and Definition of its Development Roadmap", *9th European Conference for Aeronautics and Space Sciences (EUCASS)*, 2022.

[5] S. Singh, S. Stappert, L. Bussler, M. Sippel, Y. C. Kucukosman, S. Buckingham, "A Full-Scale Simulation and Analysis of Formation Flight during In-Air Capturing", IAC-21-D2.5.2, *72nd International Astronautical Congress (IAC)*, 2021.

[6] S. Singh., S. Stappert, S. Buckingham, S. Lopes, Y.C. Kucukosman, M. Simioana, M. Pripasu, A. Wiegand, M. Sippel, P. Planquart, "Dynamic Modelling and Control of an Aerodynamically Controlled Capturing Device for 'In-Air-Capturing' of a Reusable Launch Vehicle", *11th International ESA Conference on Guidance, Navigation & Control Systems*, 2021.

[7] S. Singh, L. Bussler, S. Stappert, S. Callsen, S. Lopes, S. Buckingham, "A Superposition Approach to Aerodynamic Modelling of a Capturing Device used for In-Air Capturing of a Reusable Launch Vehicle", *9th European Conference for Aeronautics And Space Sciences (EUCASS)*, 2022.

[8] S. Singh, L. Bussler, S. Stappert, M. Sippel, C. Y. Kucukosman, S. Buckingham, "Simulation and Analysis of Pull-Up Manoeuvre during In-Air Capturing of a Reusable Launch Vehicle", *9th European Conference for Aeronautics And Space Sciences (EUCASS)*, 2022.

[9] M. Sippel, J. Klevanski: "Progresses in Simulating the Advanced In-Air-Capturing Method", *5th International Conference on Launcher Technology, Missions, Control and Avionics*, 2003.

[10] H. Pawel, K. Fritzkowski, "A Discrete Model of a Rope with Bending Stiffness or Viscous Damping", *Acta Mechanica Sinica*, pages 108–113, 2011.

[11] P. Fritzkowski, H. Kaminski, "Dynamics of a Rope Modeled as a Multibody System with Elastic Joints," *Computational Mechanics*, vol. 46, pp. 901-909, 2010.

[12] J. H. Lee, K. Ludvig, W. L. Chun, "A Method for Improving the Dynamic Simulation Efficiency of Underwater Flexible Structures by Implementing Non-Active Points in Modelling", *ICES Journal of Marine Science 65*, no. 9, 1552-1558, 2008.

[13] HyperTEN, Technical Fiber Rope, https://www.teufelberger.com/en/hyperten-technical-fiber-rope.html, last accessed: 2 June, 2022.

[14] H. L. Stein, "Ultra High Molecular Weight Polyethylene (UHMWPE)," *Engineering Materials Handbook*, 1988.

[15] L. Meirovitch, "Fundamentals of Vibrations", Waveland Press, 2010.

[16] A. de Cheveigné, and I. Nelken, "Filters: When, Why, and How (not) to Use Them", *Neuron*, 102(2), 280-293, 2019.